Magnetic and high-frequency EPR studies of an octahedral Fe(III) compound with unusual zero-field splitting parameters†

Alejandro Solano-Peralta,[a] Juan P. Saucedo-Vázquez,[a] Roberto Escudero,[b] Herbert Höpfl,[c] Hassane El-Mkami,[d] Graham M. Smith[d] and Martha E. Sosa-Torres*[a]

Received 15th August 2008, Accepted 11th November 2008
First published as an Advance Article on the web 22nd January 2009
DOI: 10.1039/b814225d

Temperature-dependent magnetic susceptibility and multi-frequency EPR (9.4, 34.5, 94 and 188 GHz) spectroscopic measurements have been carried out together with an X-ray study at 100 K to study $[Fe(DMSO)_6](NO_3)_3$. The iron(III) ion remains high-spin ($S = 5/2$) in the temperature range studied, therefore, the EPR data were interpreted using the conventional $S = 5/2$ spin Hamiltonian. A full analysis of EPR spectra at 95 GHz of a powdered sample at 290 K revealed that they are extremely sensitive to D and E values. The zfs parameters were precisely determined: $D = +0.1730$ cm^{-1}, $E = 0.00$ cm^{-1} and $\lambda = |E/D| = 0.00$. A sequence of the spectra neatly shows that the compound has a clear magnetic dependence on temperature. The study at 5 K, showed that the zfs parameters increase: $D = +0.1970$ cm^{-1}, $E = 0.017$ cm^{-1} and $\lambda = |E/D| = 0.086$. These data indicate that as the temperature decreases the D tensor increases slightly showing an increase in the rhombicity. These results confirm that $|2D| \cong h\nu$ at X-band in this case. Additionally, it has been shown by X-ray crystal analysis of $[Fe(DMSO)_6](NO_3)_3$ at 100 K that this is involved in a hydrogen bonding network, consisting of C–H···O interactions between the nitrate anions and the methyl groups of the coordinated DMSO molecules, thus suggesting that the differences found in the spectroscopic parameters D and E at different temperatures must be due to these supramolecular interactions.

1. Introduction

Iron has been widely used in coordination,[1] bioinorganic[2] and materials[3] chemistry. A large and important class of substances containing iron often shows octahedral environments. High-spin (hs) Fe(III) ($S = 5/2$) is an important magnetic state in this type of systems. Although EPR represents one of the best methods in spectroscopy to determine the electronic properties of such paramagnetic compounds, it is relatively difficult to investigate Fe(III) by conventional EPR spectroscopy, because in this oxidation state, it shows zero-field splitting (zfs) parameters in the weak or high field. Thus, the g value is expected to be close to the free-electron value of 2.0023 and frequently only two resonance signals at $g \approx 4.3$ and $g \approx 2$ have been reported.[4] In some cases, when rhombic environments are present, resonances near $g \approx 6$ and $g \approx 9$ are also observed.[5–8] However, few examples are documented for the intermediate case, where $|2D| \cong h\nu$.

A recent, exciting development in EPR spectroscopy is high-field EPR (HF-EPR) that operates at frequencies higher than 90 GHz. Thus, in systems of hs Fe(III), zfs can be measured more accurately in order to get more precise electronic information and so to correlate with the geometry and the reactivity of these complexes.[9–14]

Moreover, HF-EPR has proved to be a powerful tool to discriminate single-ion properties, due to the extreme specificity of this spectroscopy for the valence state.[15]

As part of our research program on magnetic properties (electron paramagnetic resonance and magnetic susceptibility) of coordination compounds, we describe herein the magnetic behaviour, a multi-frequency EPR study and the low temperature X-ray crystal structure of $[Fe(DMSO)_6](NO_3)_3$.

2. Experimental

2.1 Synthesis

$[Fe(DMSO)_6](NO_3)_3$ was synthesized following the literature method described by Langford.[16] Electronic absorption spectra were measured on a Hewlett Packard 8452 Diode Array spectrophotometer. Infrared spectra were obtained from KBr pellets using a Perkin-Elmer model 1600 FTIR spectrometer. Elemental analyses were performed by a microanalyser Fisons Instruments EA1108. Calcd (found) for $C_{12}H_{36}N_3O_{15}S_6Fe$: C 20.35 (20.30), H 5.09 (5.11), N 5.85 (5.91) and S 27.61 (27.10)%. Crystals suitable for X-ray analysis were obtained by a slow evaporation from a concentrated solution of the recrystallised compound.

2.2 X-Ray crystallography

X-Ray diffraction studies were performed on a Bruker-AXS diffractometer with a CCD area detector ($\lambda_{MoK\alpha} = 0.71073$ Å,

[a]*Departamento de Química Inorgánica y Nuclear, Facultad de Química, Universidad Nacional Autónoma de México, México D.F., 04510, México. E-mail: mest@servidor.unam.mx; Fax: +52 55 5616 2010*
[b]*Instituto de Investigación en Materiales, Universidad Nacional Autónoma de México, México D.F., 04510, México*
[c]*Centro de Investigaciones Químicas, Universidad Autónoma del Estado de Morelos, Ave. Universidad 1001, Cuernavaca, Morelos, 62209, México*
[d]*School of Physics and Astronomy, University of St-Andrews, Fife, Scotland, UK*

† CCDC reference number 659005. For crystallographic data in CIF or other electronic format see DOI: 10.1039/b814225d

monochromator: graphite). Frames were collected at $T = 100$ K *via* ω and ϕ–rotation ($\Delta/\omega = 0.3°$) at 10 s per frame (SMART).[17a] The measured intensities were reduced to F^2 and corrected for absorption with SADABS (SAINT-NT).[17b] Corrections were made for Lorentz and polarization effects. Structure solution, refinement and data output were carried out with the SHELXTL-NT program package.[17c,d] Non-hydrogen atoms were refined anisotropically. C–H hydrogen atoms were placed in geometrically calculated positions using a riding model (0.95 Å). Hydrogen bonding interactions in the crystal lattices were calculated by MERCURY.[18] Restraints (DFIX, DANG and EADP) have been used in order to define the geometry for the disordered nitrate ions.

2.3 Magnetic studies

These measurements were obtained using a Gouy–Evans modified magnetic balance at room temperature (290 K) and the set-up was calibrated with $Hg[Co(SCN)_4]$ as standard. A SQUID MPMS-5 Quantum Design Magnetometer was used for measuring the magnetic susceptibility as a function of temperature (2–300 K), whereby the sample for the study was prepared by encapsulating the powder in a transparent nonmagnetic resin. In all cases the χ_M values have been corrected for diamagnetism, χ_{Mdc}.

2.4 EPR measurements

EPR spectra were recorded on polycrystalline samples with a Bruker Elexsys E500 spectrometer using the X-band (9.45 GHz) and Q-Band (34.0 GHz) microwave frequencies operating at 100 kHz. The X-band EPR at low temperature was performed using an Oxford liquid helium continuous flow cryostat. The g values were determined by measuring the magnetic field, H, and the microwave frequency. High-field EPR studies (at 94 and 188 GHz) were carried out in a novel quasi-optical induction mode spectrometer at the University of St. Andrews, UK.

All spectra were simulated with the SIM program written by Weihe.[19] This program also takes into account the Boltzmann distribution factor in calculating transition probability and signal intensity. Although fairly simple, the SIM program proved to be quite efficient for the simulation of high-field spectra due to the lack of any restraint in the allowed range, not only for the spin Hamiltonian interactions, but also for the experimental parameters, in particular the magnetic field and frequency.

3. Results and discussion

3.1 X-Ray crystallography

The crystal structure of $[Fe(DMSO)_6](NO_3)_3$ has been previously analysed by Tzou *et al.*[20] showing that the iron(III) atoms have an approximate octahedral $\{FeO_6\}$ coordination geometry [Fe–O = 2.020 (2) Å, O–Fe–O angles bond = 87.40 (9) and 92.60 (9)°]. Within the crystal lattice, one of the nitrate ions is located next to DMSO ligand, while for the second nitrate ion the disorder could not be defined from the set data obtained at that time. Since the 3D structural organization influences the paramagnetic properties of the metal centres, data for the title compound were collected now at $T = 100$ K, which permitted to model a reasonable structure for the disordered nitrate ion[21] and analyse with more detail the intermolecular interactions present in the crystal lattice. In Table 1, a comparison of the geometric parameters for the two structures is shown, and the data reported for $[Fe(DMSO)_6]Br_3$[22] have also been included.

Table 1 Comparison of the crystallographic data of the $[Fe(DMSO)_6]^{3+}$ cations in compounds $[Fe(DMSO)_6](NO_3)_3$ and $[Fe(DMSO)_6]Br_3$

	$[Fe(DMSO)_6](NO_3)_3$	$[Fe(DMSO)_6](NO_3)_3$	$[Fe(DMSO)_6]Br_3$
T/K	100	294	294
Bond lengths/Å			
Fe1–O1	2.0006(15)	2.020(2)	2.000(2)
S1–O1	1.5426(16)	1.536(2)	1.543(2)
S1–C1	1.777(2)	1.759(4)	1.766(4)
S1–O2	1.771(2)	1.763(4)	1.771(4)
N1–O2	1.2487(17)	1.221(3)	—
N2–O3	1.2465(9)	1.261(9)	—
Bond angles/°			
O1–Fe1–O1^{ia}	92.46(6)	92.60(9)	92.01(7)
O1–Fe1–O1^{iia}	87.54(6)	87.40(9)	87.99(7)
O1–S1–C1	104.93(11)	104.0(2)	104.2(2)
O1–S1–C2	103.05(11)	102.7(2)	103.2(2)
C1–S1–C2	99.65(12)	99.4(2)	98.9(2)
Fe1–O1–S1	123.73(9)	124.3(1)	124.9(2)

^{a} Symmetry codes: (i) $\frac{2}{3} + x, \frac{1}{3} + y, \frac{1}{3} + z$; (ii) $\frac{2}{3} - y, \frac{1}{3} + x - y, \frac{1}{3} + z$.

The analysis of the crystal structure measured at $T = 100$ K shows that, as $T = 294$ K, the octahedral iron(III) center is located at a site of symmetry (Fig. 1).

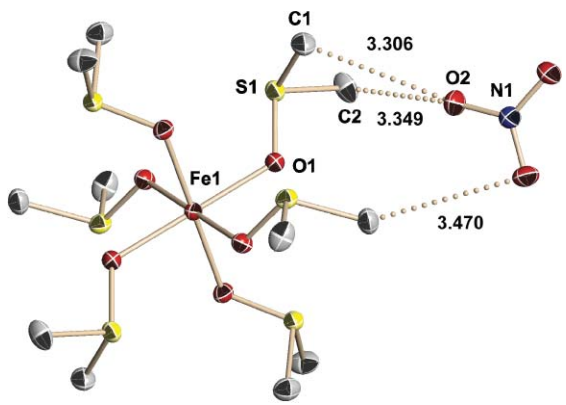

Fig. 1 The molecular structure of the $[Fe(DMSO)_6](NO_3)^{2+}$ cation present in the crystal lattice of $[Fe(DMSO)_6](NO_3)_3$ at 100 K, showing their interaction with their nitrate ions, 50% probability ellipsoids.

The nitrogen atoms of the NO_3^- anions are located also at $\bar{3}$-inversion axes, however, there are two different spatial orientations: one part is oriented perpendicular to the $\bar{3}$-axes (occupancy = 2/3), giving a ordered structure with perfect D_{3h} point group symmetry, and the second part is involved in a disordered with six different orientations (occupancy = 1/3), in accordance to the prediction of Tzou *et al.*[20] The nitrate ions participate in a series of weak C–H···O interactions with the methyl groups of the coordinated DMSO molecules. These intermolecular contacts range from 2.77 to 3.51 Å (C···O distances) and are all within the limits established previously for a large series of crystal

structures,[23] *e.g.* in the case of the ordered anions there are four interactions in the range of 2.40–2.58 Å (C···O: 3.306(4)–3.495(3) Å, 150–155°).

3.2 Magnetic studies

The yellow-orange crystals of $[Fe(DMSO)_6](NO_3)_3$ (290 K) change slightly to a very pale yellow colour as the temperature of the magnetic measurements was decreased to ≈ 77 K. For the effective magnetic moment, a value of $\mu_{eff} = 5.98$ BM was found at 290 K, that is very close to the spin-only value for a $S = 5/2$ systems.[24] The magnetic susceptibility *vs.* temperature (2–300 K) shows a Curie–Weiss behaviour with a weak antiferromagnetic coupling ($\theta = -0.2576$ K). The magnetic moment obtained at 300 K is maintained within temperature range explored (Fig. 2), showing that the iron(III) remains high-spin ($S = 5/2$).

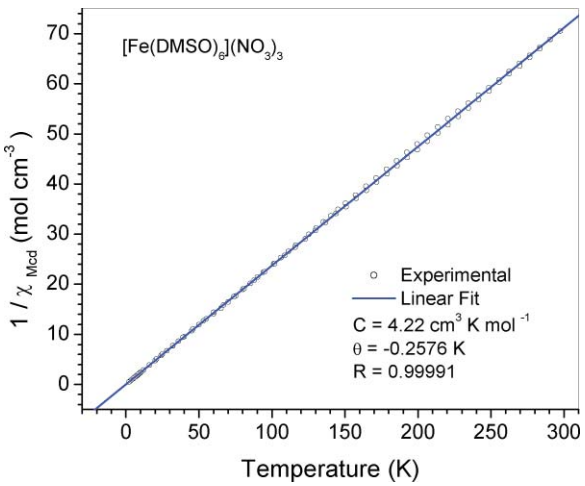

Fig. 2 Plot of $1/\chi$ Mdc (○) *vs.* T for $[Fe(DMSO)_6](NO_3)_3$.

3.3 EPR measurements

In order to obtain more information about the magnetic behaviour out of the sample, EPR spectra were recorded at several temperatures (290–5 K) as shown in Fig. 3. Although the EPR spectrum of this compound was already published this was done in solution at room temperature and only at X-band.[25]

The spectrum at room temperature shows well defined lines from 0–8000 G with very weak signals around 10 500 G and no hyperfine interactions, since iron has a non-magnetic nucleus. All the spectra may be described with $g_{iso} \cong g_e$[26] since high-spin Fe(III) is a species with five unpaired electrons in the 3d shell. Therefore, the total angular moment is zero and, the ground state is ^6S.[6] The spin-Hamiltonian that describes these spectra is typical for $S = 5/2$ systems:

$$\hat{H} = g\beta BS + D\left(S_z^2 - \frac{1}{3}S(S+1)\right) + E\left(S_x^2 + S_y^2\right)$$

where the first term corresponds to the electronic Zeeman and the second and third terms correspond to the zero-field splitting (zfs) parameters with D and E referred to as the axial and rhombic components, because they remove the degeneracy of energy states independent of the magnetic field. It has been assumed that the

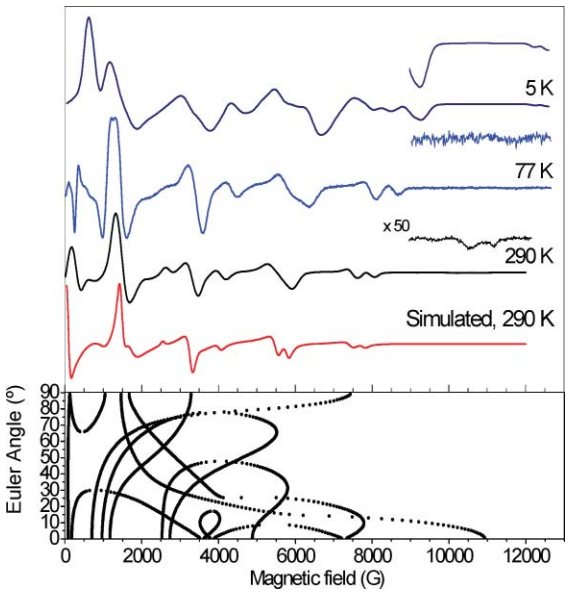

Fig. 3 X-Band EPR spectra at different temperatures and simulated powder EPR spectra of $[Fe(DMSO)_6](NO_3)_3$ at 290 K (top). Diagram of angular dependence of the resonance lines for a $S = 5/2$ species (bottom).

principal axes of the g, D and E tensors are parallel with the molecule axes, too.[27]

According to Mabbs and Collison,[28] this type of spectrum can be attributed to a high-spin Fe(III) species with axial distortion where $2D \cong h\nu$. Under this situation it is possible to observe a large number of signals in a wide range of magnetic field, including close to zero, and off-axis signals (looping transition). These signals are of particular importance when the powder spectra are considered,[29] since they correspond to non-continuous resonance lines in the range considered of θ and ϕ, this means that the resonance lines are closed transitions that generate signals off the axis and this results in state-mixing and the observation of forbidden transitions. Thus, most of the strongest features could be associated to perpendicular or off-axis transitions. For this reason, it is not easy to observe any resonance at $g = 2.0$, because it could be lost in the envelope of an adjacent more intense signal at $g_{eff} = 2.17$.

At lower temperatures, the overall spectrum changed, concerning the number of lines, their relative intensities and their resonant fields, suggesting that the zfs parameters vary as the temperature is lowered, This also indicates that the hs Fe(III) species are maintained at low temperature, which is in agreement with the magnetic measurements as a function of temperature.

Thus, as the temperature decreases, the spectra show a splitting and a shifting of the outmost signals (near 8000 G) and the weaker outer signal (11 000 G) to the highest field, and provide a fingerprint of a rhombic distortion. These findings indicate a change in the zfs parameters as the temperature decreases, which could be associated with a distortion in the xy plane (diagram of angular dependence in Fig. 3). Additionally, a relevant increase in the intensity of the lines is observed, in particular at 5 K. The low-field lines (800 G) show a bigger increase in the intensity. The effect of increasing the intensity of the signals as the temperature decreases are determined by the Boltzmann distribution of the energy levels involved. Thus, the variations of the line intensity, allow a

determination of the sign of the D parameter.[30,31] However, it is not possible to determinate the sign of the axial fine-structure parameter without ambiguity, because at low temperature $E \neq 0$ is feasible and a mix of orbitals could emerge producing an increase in the intensity of some signals.[32] Thus, under these conditions, the X-band EPR spectra are very complex and hardly interpretable, but it indicates that zfs parameters are not neglected, $|2D| \approx g\beta B$.

A similar situation holds for the Q-band (34 GHz) frequency (Fig. 4). The main spectral features consist of six prominent signals with effective g values of 2.752, 2.358, 2.044, 1.930, 1.856 and 1.791 and several weak signals at low field (9.133, 5.465, 3.519 and 2.946). All g values are out of the expected range for hs Fe(III) species,[28] and as in the previous case, the Q-band spectrum is representative of an intermediate field regime where zfs terms are comparable to the electronic Zeeman factor, $|2D| \approx g\beta B$, and no simple pattern of the EPR spectra is obtained.

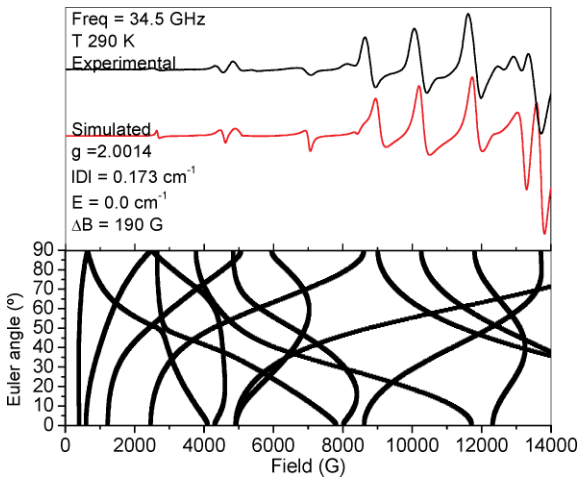

Fig. 4 Experimental and simulated Q-band EPR spectra of a powder sample of $[Fe(DMSO)_6](NO_3)_3$ at 290 K (top). Diagram of the angular dependence of the resonance lines for a $S = 5/2$ species (bottom).

In the high-field regime, in principle, for the $S = 5/2$ the condition limit $g\beta B >> |D|$ is satisfied and symmetric spectra centred at approx. $g = 2.00$ are expected. Furthermore, the resonance lines appear with better resolution and, therefore, the HF-EPR spectrum will be much simpler than that of the X-band.[30] This is a great advantage since the spectra are more easily calculated and readily interpreted when a first-order spectrum is observed. In addition, a better resolved g anisotropy is also obtained. Under these conditions, it is possible to separate "forbidden" ($\Delta M_s = \pm 2$, ± 3) from "allowed" ($\Delta M_s = \pm 1$) transitions and EPR signals will show linear behaviour with a slope proportional to an effective g factor.[30,33] This is shown in Fig. 5, in which the transition energy for each feature is plotted *versus* resonance field.

The W-band (94 GHz) spectrum at 290 K (see Fig. 6) consists of seven lines with starting intensity decreasing from the centre towards the sides, The intense doublet, centred at 3.35 T ($g = 2.014$), corresponds to the resonant field of Fe(III) in a cubic symmetry. The central doublet is surrounded by two weaker broad lines, at 3.14 and 3.50 T, two outer doublets, at 2.93 and 3.76 T, and two very weak signals at 2.49 and 4.19 T. As expected, no hyperfine structure is detected due to the low abundance of ^{57}Fe and the presence of intermolecular dipole–dipole interactions.

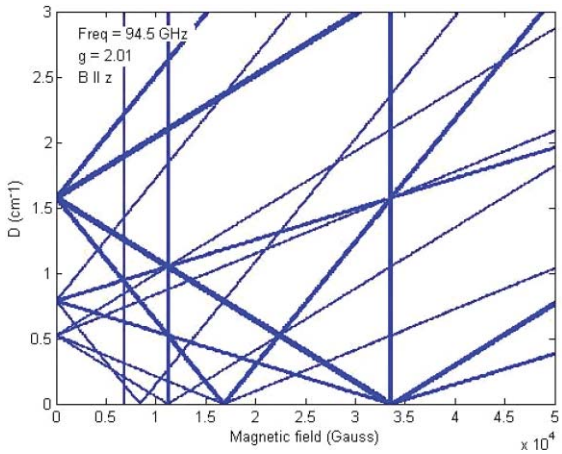

Fig. 5 Plot of transition energy *vs.* resonance field for hs Fe(III) using the spin Hamiltonian with $S = 5/2$ and $g_{iso} = 2.01$.

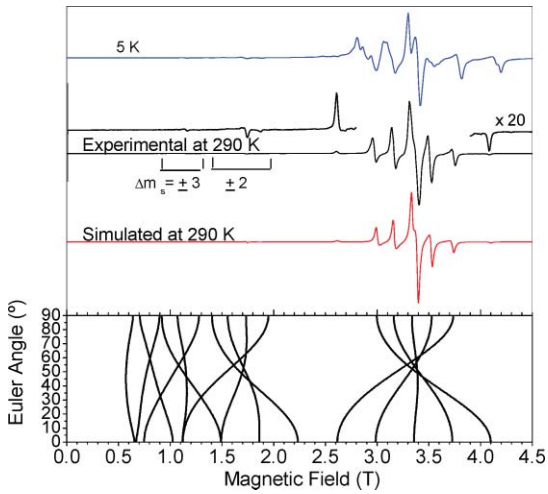

Fig. 6 (top) Experimental and simulated W-band EPR spectra, at several temperatures, and (bottom) diagram of angular dependence of the resonance lines of $[Fe(DMSO)_6](NO_3)_3$ with the parameters in the text and isotropic Gaussian linewidth of 190 G at 290 K.

Although all EPR spectra were explained in terms of a hs Fe(III) system, some comments are needed: firstly, regarding the number of signals, only five are expected for $S = 5/2$ systems with E/D equal or close to 0 or 1/3,[28] whereas for intermediate $|E/D|$ ratios, up to 13 transitions are expected in a isotropic case, see Fig. 7.

In this case, the spectrum obtained at 290 K shows seven signals, which indicates that the axial parameter is different from zero ($D \neq 0$ and $E = 0$ cm^{-1}). Five signals are associated to transitions along the z axes, Fig. 5, and the additional two signals are due to the angular dependence and the signal line-width.[28,31] Thus, the position of the signals, when the Euler angle in the diagram of angular variation (θ) is zero, is different when the θ value is near or close to 90° (x and y magnetic axes). Similar effects have been found in other d^5 systems.[34]

The second point to note is the splitting of the central signal (3.32 T) that is assigned to a $|-1/2\rangle \rightarrow |1/2\rangle$ transition along z. This split signal is in contradiction with the very small g anisotropy determined for other compounds by EPR[35] or magnetic measurements.[36] In the case of hs Fe(III) (d^5, $S = 5/2$), the

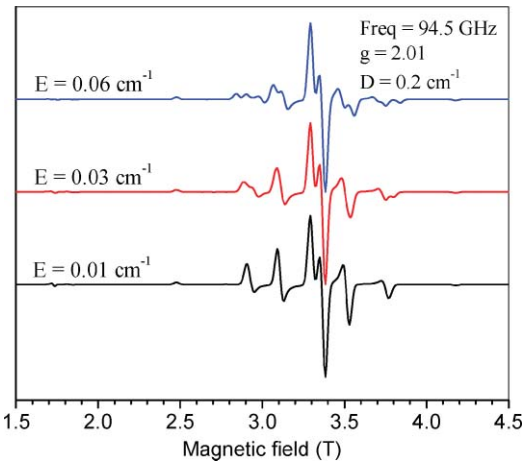

Fig. 7 Simulated powder W-band EPR (94 GHz,) spectra, at 290 K in a rhombic field; $g = 2.01$, $|D| = 0.2$ cm^{-1} and $E \neq 0.0$ cm^{-1}.

anisotropy of the Zeeman interaction is considered small or negligible due to the large gap between the ground state and the first excited state.[31,35] However, this splitting could be due to its angular dependence on the D parameter.[37] This effect produces that g_z generates a very weak signal by its low contribution that is difficult to observe, and additional signals that could be assigned to the transitions of microcrystalline in the xy plane (Euler angle equal to 90° in Fig. 8), and the other could be to respond of the sample to middle angles (Euler angle equal to 41.2° and denoted by an asterisk in the spectra in Fig. 8).[30]

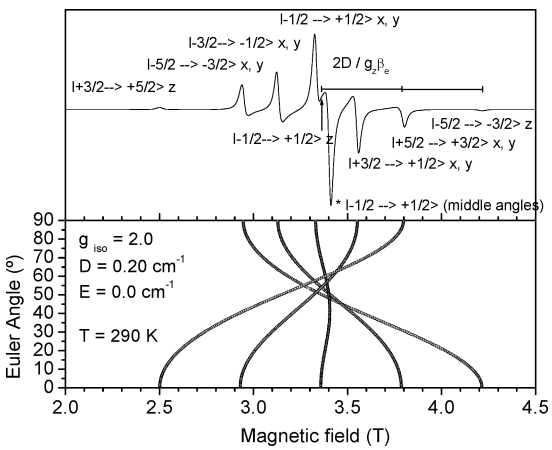

Fig. 8 Position of the signals ($\Delta M_s = \pm 1$) in the powder HF-EPR (ν = 94.0 GHz) spectrum in an axial field; $g = 2.00$, $D = +0.2$ and $E = 0.0$ cm^{-1} at 290 K. Transitions (*) in the plane xy and (**) in middle orientations.

A calculation was performed to simulate the W-band spectra, using the same set of parameters used for the simulation of the X-band spectrum. The comparison of the spectra (experimental and simulated at 290 K in Fig. 6) shows that the main lines are well reproduced. Therefore, the peculiar X-band spectrum is caused by the D zfs parameter, which is fully comparable with the magnitude of the Zeeman interaction, $|2D| \cong h\nu$ at 9.5 GHz.

The registered W-band EPR (94 GHz) spectra of the sample at 5 and 290 K are shown in Fig. 6, as a first derivative of radiation absorption *vs.* the applied magnetic field (T).

Similar changes in the spectra at X-band and W-band were observed at 5 K. Several signals, shifted and changed their relative intensities from the those at 290 K due probably to different zfs parameters, suggesting a rhombic distortion at low temperature. This means that the x and y magnetic axes should be different and therefore a splitting and shifting of the signals should be observed. This effect is mainly observed in the lateral signals that are split, while the central signal remains almost intact. On the other hand, some signals at the left of the central signal are more intense that their corresponding signals at the right. Moreover, the signal at 4.19 T can be assigned to a $|-5/2> \rightarrow |-3/2>$ transition which is more intense that the signal at 2.49 T that is assigned to the $|5/2> \rightarrow |3/2>$ transition. This allows to determine the sign of the zfs parameter D. If the zfs interaction is taken positive, then the intensity of the signal for $D > 0$ can be understood by taking into account the calculated energy-level diagrams in Fig. 9, where the particular line corresponds to the transition connecting states of the lowest energy. If the sign of D would be negative, this level would be the highest in energy and, hence, this transition has to be thermally activated and should be detectable at elevated temperatures only. So, together with two simulated spectra: one calculated using a negative value of $D = -0.173$ cm^{-1}; the other a positive value of the same magnitude but both with the same E value, $E = 0.017$ cm^{-1} in Fig. 10. It is evident that a much better agreement between the experiment and simulation is obtained for the case of positive D parameter.[11,28]

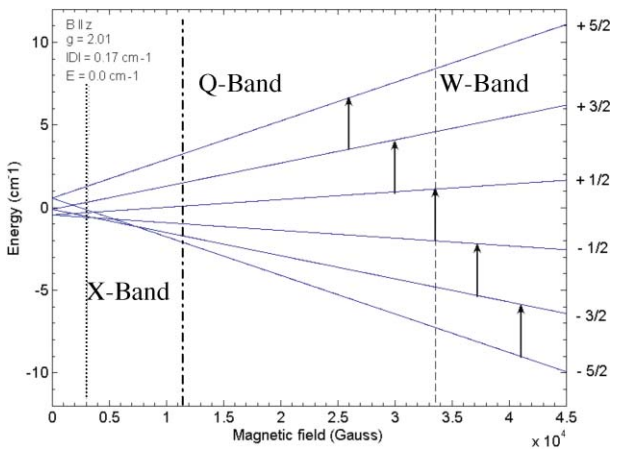

Fig. 9 Plot of the energy *vs.* field for the six energy levels arising from an $S = 5/2$ spin state with $g = 2.01$ that is split by zfs where $|D| = 0.17$ and $E = 0.0$ cm^{-1}. A dotted vertical line indicates the energy corresponding at X-band, a dot-dashed line for Q-band while a dashed line for W-band. Vertical arrows indicate the expected transitions at 94 GHz.

The final values of best-fit spin Hamiltonian parameters of $Fe(DMSO)_3](NO_3)_3$ show that almost all main lines are well reproduced. These are given in Table 2.

The shape of the W-band spectra for a classical powder pattern, where all orientations are statistically realized, is not obtained at low temperature. This could be due to individual EPR signals from microcrystallines that the strong magnetic field moves in preferential orientations. This effect would result from powder pattern having not a sufficient number of random-orientation single crystals.

Table 2 Results of the best fit EPR spectra involving zfs parameters for polycrystalline powder of $[Fe(DMSO)_6](NO_3)_3$ at variable temperature

Temperature/K	g	D/cm^{-1}	E/cm^{-1}	$\lambda/(E/D)$
290	2.014	+0.1730	0.0	0.0
77	2.014	+0.1894	0.003	0.016
5	2.014	+0.1970	0.017	0.086

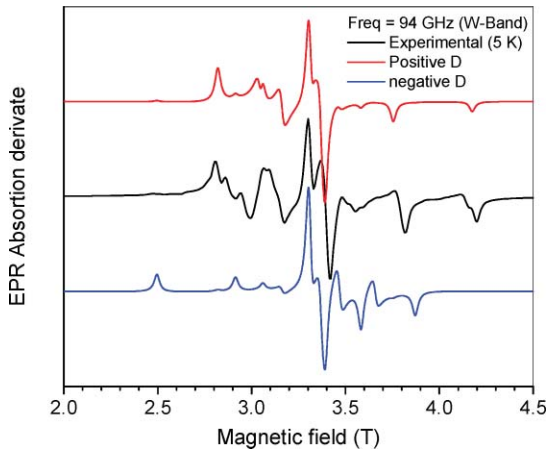

Fig. 10 Determining the sign of D: low-temperature experimental HF-EPR spectrum of $[Fe(DMSO)_6](NO_3)_3$ complex (solid line, center) and simulations using the values $D = +0.197$ cm^{-1} (top) and -0.193 cm^{-1} (bottom), each with $E = 0.017$ cm^{-1}. Parameters: temperature, 5 K; frequency, 93.9 GHz.

At the G-band (188 GHz), Fig. 11, HF-EPR spectra was obtaining, too, and it shows again seven signals around $g = 2.014$ at 290 K, but now the central signal appears more defined. In this case, the condition $g\beta B >> |D|$ is also satisfied and, therefore, the spectrum is very simple and easy to interpret.

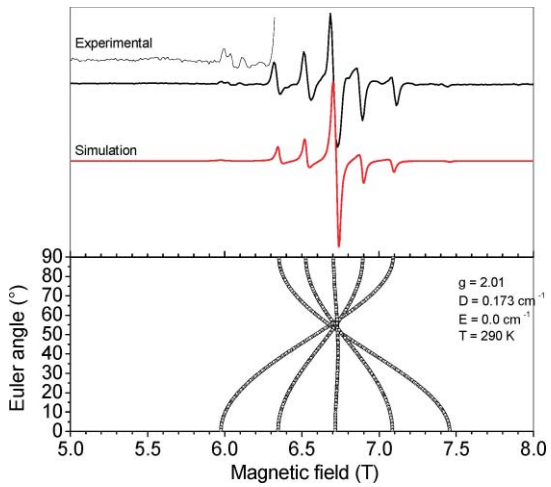

Fig. 11 (Top) Experimental and simulated G-band HF-EPR spectra at 290 K of $[Fe(DMSO)_6](NO_3)_3$, and (bottom) diagram of angular dependence of the resonance with the parameters in the text and isotropic Gaussian linewidth of 190 G.

The only difference between the W-band spectra and the spectra obtained at the G-band is the very weak splitting of the signals that could be due to the almost null effect of the D term. The shape must be similar since the zfs parameters that govern EPR spectra are field-independent and the resonance field is simply shifted as $B' = Bv'/v$, where B and B' are the field locations of the same line at v and v', respectively.

The best-fit parameters are equal to the obtained at W-band EPR and they are show in Table 2 demonstrating that, in this case, the energy used by conventional EPR (at X-band) is comparable to the zfs parameters of this complex.

Finally, the differences found in the D and E values at lower temperatures for this compound can be attributed to supramolecular interactions in this case to the hydrogen bonding as it has been recognized that these types of interactions are responsible for magnetic properties in the solid-state.

4. Conclusions

The high-field approach allowed to determinate the absolute value and positive sign of the axial fine-structure parameter for this polycrystalline compound without ambiguity and even superior accuracy as compared to the studies at the X- and Q-band frequencies, confirming the condition of $|2D| \cong h\nu$ at the X-band. This is due to the fact that zfs values for this compound at high fields can accurately be determined *via* first-order effects.

By magnetic studies, we have shown that the spin of Fe(III) $S = 5/2$ is maintained from 300–2 K. So, the change in morphology of the EPR spectra of $[Fe(DMSO)_6](NO_3)_3$ obtained at different temperatures, from 290–5 K in the solid-state it is due to the increased rhombicity as the temperature is lowered.

We have shown, by crystal analysis, that although the molecular structure of the cation is practically the same at 100 and 290 K, the compound is involved in a hydrogen bonding network, consisting of C–H···O interactions between the nitrate anions and the methyl groups of the coordinated DMSO molecules. Thus, it is suggested that the differences in the spectroscopic parameters, D and E at different temperatures in the multi-frequency (X, Q, W and G-band) EPR study found for the compound are attributed to these supramolecular interactions.

Acknowledgements

M. E. S. T. and A. S. P. are grateful to DGAPA-UNAM (research project IN210108) and to CONACYT (research project 41128-Q) for financial support, R. E. thanks DGAPA-UNAM (research project IN101107). We also thank Dr H. Weihe (H. C. Ørsted Institute, University of Copenhagen, Denmark) for the EPR simulation software and finally to USAI (Unidad de Servicios de Apoyo a la Investigación, Facultad de Química) for the analytical services.

Notes and references

1 (*a*) M. V. Twigg and J. Burgess, in *Comprehensive Coordination Chemistry II; From Biology to Nanotechnology*, ed. J. A. McCleverty and T. J. Meyer, Elsevier, Amsterdam, 2005, vol. 5, ch. 5.4, pp. 403–553; (*b*) W. Macyk, A. Franke and G. Stochel, *Coord. Chem. Rev.*, 2005, **249**, 2437.

2 (*a*) E. I. Solomon, T. C. Brunold, M. I. Davis, J. N. Kemsley, S.-K. Lee, N. Lehnert, F. Neese, A. J. Skulan, Y. S. Yang and J. Zhou, *Chem. Rev.*, 2000, **100**, 235; (*b*) J. J. R. Frausto Da Silva and R. J. P. Williams, *The Biological Chemistry of the Elements: The Inorganic Chemistry of Life*, Oxford University Press, Oxford, 2001, ch. 12–13, pp. 341–399; (*c*) R. R. Crichton, *Inorganic Biochemistry of Iron Metabolism: From*

Molecular Mechanisms to Clinical Consequences, John Wiley & Sons, Ltd., Chichester, 2001.
3 (*a*) X. H. Wang, J.-G. Li, H. Kamiyama, M. Katada, N. Ohashi, Y. Moriyoshi and T. Ishigaki, *J. Am. Chem. Soc.*, 2005, **127**, 10982; (*b*) M. Granström and O. Inganas, *Adv. Mater.*, 1995, **7**, 1012; (*c*) R.-A. Eichel, H. Meštrić, K.-P. Dinse, A. Ozarowski, J. van Tol, L. C. Brunel, H. Kungl and M. J. Hoffmann, *Magn. Reson. Chem.*, 2005, **43**, S166; (*d*) H. Meštrić, R.-A. Eichel, K.-P. Dinse, A. Ozarowski, J. van Tol and L. C. Brunel, *J. Appl. Phys.*, 2004, **96**, 7440.
4 R. Berger, J. Kliava, E. Yahiaoui, J. C. Bissey, P. K. Zinsou and P. Beziade, *J. Non-Cryst. Solids*, 1995, **180**, 151.
5 G. Palmer, Electron Paramagnetic Resonance in Metalloproteins in *Physical Methods in Bioinorganic Chemistry: Spectroscopy and Magnetism*, ed. L. Que, University Science Books, Sausalito, California, 2000, ch. 3, pp. 121–186.
6 A. Bencini and A. Gateschi, in *Inorganic Electronic Structure and Spectroscopy; Methodology*, ed. E. I. Solomon and A. B. P. Lever, Wiley-Interscience, 1999, ch. 2, pp. 93–160.
7 X. Hu and K. Meyer, *Inorg. Chim. Acta*, 2002, **337**, 53.
8 A. M. Ferretti, A.-L. Barra, L. Forni, C. Oliva, A. Schweiger and A. Ponti, *J. Phys. Chem. B*, 2004, **108**, 1999.
9 (*a*) P. J. M. van Kan, E. von der Horst, E. J. Reijerse, P. J. M. van Bentum and W. R. Hagen, *J. Chem. Soc., Faraday Trans.*, 1998, **94**, 2975; (*b*) D. Arieli, D. E. W. Vaughan, K. G. Strohmaier, H. Thomann, M. Bernardo and D. Goldfarb, *Magn. Reson. Chem.*, 1999, **37**, S43; (*c*) J. Telser, J. van Slageren, S. Vongtragool, M. Dressel, W. M. Reiff, S. A. Zvyagin, A. Ozarowski and J. Krzystek, *Magn. Reson. Chem.*, 2005, **43**, S130.
10 (*a*) K. K. Andersson and A.-L. Barra, *Spectrochim. Acta, Part A*, 2002, **58**, 1101; (*b*) J. Krzystek, A. Ozarowski and J. Telser, *Coord. Chem. Rev.*, 2006, **250**, 2308.
11 K. K. Andersson, P. P. Schmidt, B. Katterle, K. R. Strand, A. E. Palmer, S. K. Lee, E. I. Solomon, A. Gräslund and A. L. Barra, *JBIC, J. Biol. Inorg. Chem.*, 2003, **8**, 235.
12 F. Di Benedetto, G. Andreozzi, G. Baldi, A. Barzanti, G. P. Bernardini, V. Faso, L. A. Pardi and M. Romanelli, *J. Eur. Ceram. Soc.*, 2006, **26**, 2301.
13 F. Biaso, C. Duboc, B. Barbara, G. Serratrice, F. Thomas, D. Charapoff and C. Béguin, *Eur. J. Inorg. Chem.*, 2005, 467.
14 A. Solano-Peralta, M. E. Sosa-Torres, M. Flores-Alamo, H. El-Mkami, G. M. Smith, R. A. Toscano and T. Nakamura, *Dalton Trans.*, 2004, 2444.
15 P. ter Heerdt, M. Stefan, E. Goovaerts, A. Caneschi and A. Cornia, *J. Magn. Reson.*, 2006, **176**, 21.
16 C. H. Langford and F. M. Chung, *J. Am. Chem. Soc.*, 1968, **90**, 4485.
17 (*a*) *Bruker Analytical X-Ray Systems*, SMART: Bruker Molecular Analysis Research Tool, v. 5.618, 2000; (*b*) *Bruker Analytical X-Ray Systems*, SAINT + NT, v. 6.04, 2001; (*c*) G. M. Sheldrick, *SHELX-86, Program for Crystal Structure Solution*, University of Göttingen, Göttingen, Germany, 1986; (*d*) *SHELXTL-NT*, Bruker Analytical X-Ray Systems, v. 6.10, 2000.
18 *New Software for Searching the Cambridge Structural Database and Visualizing Crystal Structures*, Mercury, v. 1.4.1; I. J. Bruno, J. C. Cole, P. R. Edgington, M. Kessler, C. F. Macrae, P. McCabe, J. Pearson and R. Taylor, *Acta Crystallogr., Sect. B: Struct. Sci.*, 2002, **58**, 389.
19 C. J. H. Jacobsen, E. Pedersen, J. Villadsen and H. Weihe, *Inorg. Chem.*, 1993, **32**, 1216.
20 J.-R. Tzou, M. Mullaney, R. E. Norman and S.-C. Chang, *Acta Crystallogr., Sect. C: Cryst. Struct. Commun.*, 1995, **51**, 2249.
21 Crystal data for $[Fe(DMSO)_6](NO_3)_3$: $C_{12}H_{36}FeN_3O_{15}S_6$, $M_r = 710.65$ g mol^{-1}, $0.21 \times 0.28 \times 0.41$ mm^3, $T = 100$ K, trigonal, space group $R\bar{3}$, $a = 11.3913(6)$, $c = 19.6535(14)$ Å, $V = 2208.6(2)$ Å^3, $Z = 3$, $\rho_{calcd} = 1.60$, $\theta_{max} = 25$, 864 independent reflections ($R_{int} = 0.023$), $R_1 = 0.0302$ for 842 reflections with $I > 2\sigma(I)$ and $wR_2 = 0.0798$ for all data, 76 parameters, GOF = 1.049, $\Delta\rho_{max/min} = 0.652$ and –0.692 e Å^{-3}.
22 P. R. Martínez-Alanis, R. A. Toscano and I. Castillo, *Acta Crystallogr., Sect. E: Struct. Rep. Online*, 2005, **61**, m2179.
23 (*a*) R. Taylor and O. Kennard, *J. Am. Chem. Soc.*, 1982, **104**, 5063; (*b*) G. R. Desiraju, *Acc. Chem. Res.*, 1991, **24**, 290; (*c*) T. Steiner, *Chem. Commun.*, 1997, 727; (*d*) A. Nangia and G. R. Desiraju, *Acta Crystallogr., Sect. A: Found. Crystallogr.*, 1998, **54**, 934; (*e*) G. R. Desiraju, *Acc. Chem. Res.*, 2002, **35**, 565; (*f*) T. Steiner, *New J. Chem.*, 1998, **22**, 1099.
24 O. Kahn, *Molecular Magnetism*, VCH, Weinheim, 1993.
25 S. A. Cotton and J. F. Gibson, *J. Chem. Soc. A*, 1971, 1690.
26 O. Jiménez-Sandoval, D. Ramírez-Rosales, M. del J. Rosales-Hoz, M. E. Sosa-Torres and R. Zamorano-Ulloa, *J. Chem. Soc., Dalton Trans.*, 1998, 1551.
27 B. Mc Garvey, in *Transition Metal Chemistry; A Series of Advances*, ed. R. L. Carlin, Marcel Decker, New York, 1966, vol. 3.pp. 90–201.
28 F. E. Mabbs and D. Collison, *Electron Paramagnetic Resonance of d Transition Metal Compounds*, Studies in Inorganic Chemistry 16, Elsevier, Amsterdam, 1992.
29 (*a*) S. K. Misra, *J. Magn. Reson.*, 1999, **137**, 83; (*b*) S. K. Misra, *J. Magn. Reson.*, 1999, **140**, 179.
30 W. Weltner Jr., *Magnetic Atoms and Molecules*, Dover, New York, 1989.
31 N. M. Atherton, *Principles of Electron Spin Resonance*, Physical Chemistry Series, Ellis Horwood-Prentice Hall, New York, 1993.
32 J. R. Pilbrow, *Transition Ion Metal Electron Paramagnetic Resonance*, Oxford Science Publishers, Oxford, 1990.
33 (*a*) J. Brickmann and G. Kothe, *J. Chem. Phys.*, 1973, **59**, 2807; (*b*) S. I. Weissman and G. Kothe, *J. Am. Chem. Soc.*, 1975, **97**, 2537.
34 (*a*) C. Duboc, T. Phoeung, S. Zein, J. Pecaut, M.-N. Collomb and F. Neese, *Inorg. Chem.*, 2007, **46**, 4905; (*b*) C. Duboc, V. Astier-Perret, H. Chen, J. Pécaut, R. H. Crabtree, G. W. Brudvig and M.-N. Collomb, *Inorg. Chim. Acta*, 2006, **359**, 1541; (*c*) D. M. L. Goodgame, H. El Mkami, G. M. Smith, J. P. Zhao and E. J. L. McInnes, *Dalton Trans.*, 2003, 34.
35 G. L. Abbati, L. C. Brunel, H. Casalta, A. Cornia, A. C. Fabretti, D. Gatteschi, A. K. Hassan, A. G. M. Jansen, A. L. Maniero, L. Pardi, C. Paulsen and U. Segre, *Chem.–Eur. J.*, 2001, **7**, 1796.
36 R. Boca, *Coord. Chem. Rev.*, 2004, **248**, 757.
37 W. T. Oosterhuis, *Struct. Bonding*, 1974, **20**, 19.

